Molecular mechanism of SARS-Cov-2 components caused ARDS in murine model

Tingxuan Gu[1, 2*], Simin Zhao[2, 4*], Guoguo Jin[2, 5], Mengqiu Song[1, 2], Yafei Zhi[2], Ran Zhao[1, 2], Fayang Ma[1, 2], Yaqiu Zheng[2], Keke Wang[2], Hui Liu[1, 2], Mingxia Xin[2], Wei Han[2], Xiang Li[1, 2, 3], Christopher D Dong[6] , Kangdong Liu[1, 2, 3], Zigang Dong[1, 2+]

[1] Department of Pathophysiology, School of Basic Medical Sciences, College of Medicine, Zhengzhou University, Zhengzhou, Henan, P.R. China

[2] China-US (Henan) Hormel Cancer Institute, Zhengzhou, Henan, P.R. China

[3] Henan Provincial Cooperative Innovation Center for Cancer Chemoprevention, Zhengzhou University, Zhengzhou, Henan, P.R. China

[4]Affiliated Tumor Hospital of Zhengzhou University, Zhengzhou, Henan, P.R. China

[5]The Henan Luoyang Orthopedic Hospital, Zhengzhou, Henan, P.R. China

[6]Wartburg College, Waverly, IA, USA

[*]These authors contributed equally to this work

Corresponding Author：

Professor Zigang Dong,

Department of Pathophysiology, School of Basic Medical Sciences, College of Medicine, Zhengzhou University, Zhengzhou, Henan, China

Fax) +86-371-65587670; Phone) +86-371-65587008; E-mail) dongzg@zzu.edu.cn

Abstract: COVID-19 has become the biggest challenge to global health, and until now, no efficient antiviral agents were developed. The SARS-Cov-2 infection is characterized by pulmonary and systemic inflammation, multi-organ dysfunctions were observed in severe patients, acute respiratory distress syndrome (ARDS) and respiratory failure contribute to most mortality cases. There is an urgent need for an effective drugs and vaccines against SARS-Cov-2 and SARS-Cov-2-caused ARDS. However, most researchers cannot perform SARS-Cov-2 research or SARS-Cov-2 caused ARDS study due to lacking P3 or P4 facility. We developed a non-infectious, highly safety, SARS-Cov-2 components induced murine model to study the SARS-Cov-2 caused ARDS and cytokine storm syndrome (CSS). We explored a robust murine animal model for anti-inflammation treatment of COVID-19 to study the mechanism of ARDS and CSS caused by SARS-Cov-2. We investigated mAbs and inhibitors which are potently neutralize the pro-inflammatory phenotype from COVID-19, and find these mAbs or agents can relieve pulmonary and CSS in the lung.

Keywords: COVID-19, SARS-Cov-2, acute respiratory distress syndrome, cytokine storm syndrome

Introduction

In early December 2019, pneumonia of an unknown cause appeared in Wuhan. The virus strain was first isolated from patient samples on January 7, 2020, and the whole genome sequence of the virus was then obtained on January 10, 2019[1-3]. The genome of the virus was compared with the sequences of SARS-Cov and MERS-Cov, and the homology of the genes was found to be about 79% and 50% respectively. Importantly, the spike gene, the encoding gene of S protein that mediates the interaction between coronavirus and host cell, showed great differences. Therefore, it was named novel

coronavirus (SARS-Cov-2)[4]. The SARS-Cov-2 caused ARDS/pneumonia being named COVID-19[5]. A total of 6114, 046 confirmed cases of pneumonia caused by SARS-Cov-2 have been reported globally as of June 1st, 2020. The total number of deaths worldwide reached 373,188. Until now, no specific antiviral drugs or vaccines for SARS-Cov-2 are developed. Current control strategies are still routine, primarily by limiting social contact and isolating patients. Coronavirus has caused serious damage to public health and as such, methods to control the virus and improve the treatments have quickly become urgent issues concerning national security across the world.

Coronaviruses are RNA viruses with an envelope with a linear single-stranded and positive-sense RNA genomes inside and widely exist in nature. Approximately 2/3 of the sequence at the 5 'end of the genome is a polymerase gene that encodes the viral polymerase complex ORF1a/b; About a third of the genome at the '3' end contains many genes that encode the structural protein and accessory protein of the coronavirus. These genes have a specific sequence in their genome: 5 '-polymerase gene (replicate) -spike protein gene (S) -envelope protein gene (E) -membrane protein gene (M) -nucleocapsid protein gene (N) -3'. Coronaviruses entry into cells is primarily dependent on the spike (S) protein, where it contains 2 important function subunits, of which S1 is responsible for binding the receptor and S2 for membrane fusion. When the receptor binding domain (RBD) of S1 protein specifically binds to the corresponding site of cell surface receptor (ACE2), it induces conformational changes of S2, which causes the fusion of the virus envelope and the cellular membrane, eventually leading to the viral entry into the cells[6-8]. As the coronavirus infection progresses, patients may develop acute respiratory distress syndrome (ARDS), or even multiple organ failure (MOF)[9]. Cytokine storm syndrome (CSS) occurs when a microorganism or drug that induces a disorder of the immune system and cause a rapid increase of proinflammatory cytokine levels after the stimulus. Studies have shown that cytokine storms are

associated with the deterioration of various infectious diseases, including ARDS[10]. The formation of the CSS in COVID 19 patients occurs when the serum levels of inflammatory cytokines IL-6, IL-1β, IL-2, IL-8, IL-17, G- CSF, GM-CSF, IP10, MCP1, MIP1α and TNFα are significantly increased, recruit immune cells through a positive feedback loop, eventually forming a cytokine storm[10-13]. The CSS are an important reason for the deterioration of COVID-19 patients and blocking the cytokine storm can help reverse the condition of severe patients. However, the specific immunological mechanism of its occurrence has not yet been fully clarified. Therefore, clarifying the specific mechanism of the occurrence of cytokine storm in patients with COVID-19 and discovering the key cytokines can allow for more effective methods to block cytokine storm, which is of great significance for the treatment of COVID-19 patients.

The continued global epidemic of COVID-19 emphasizes the necessity of establishing a COVID-19 pneumonia animal model. The ideal animal model for studying COVID-19 pneumonia is one that is susceptible to pathogens and simulates the human pathophysiological process, such as acute lung injury, ARDS, and the formation of CSS. Currently, most animal models have used virus strains isolated from patients to infect mammals. This model may simulate human pathophysiological processes, but it extremely lacks biosecurity and only can perform in the biosecurity P3/P4 lab[14,15]. Furthermore, because of the strict management of virus strains, many COVID-19 research institutions are unable to construct animal models and doing COVID-19 related research. There is an urgent need to establish an effective animal model for the research of COVID-19 pneumonia that is able to be utilized in less well equipped laboratories while still staying within their biosecurity levels.

Here, our laboratory has successfully developed a pneumonia animal model that simulates the cytokine storms and the pathophysiological changes seen in the patients with COVID-19 by using Poly I:C and

SARS-Cov-2 spike protein (Poly I:C and SP). Most exciting of all, this successful mouse model is highly biosecurity and not contagious, which use a synthetic analog of a double stranded RNA (dsRNA) virus instead of highly contagious SARS-Cov-2 virus. After Poly I:C and SP induction, cytokines levels (IL-6, IL-1α, and TNF-α) and the proportion of neutrophils in mice alveolar lavage fluid increased dramatically. The induction group also showed pulmonary inflammation exudates, neutrophils infiltration and other pathological changes. In our results, mAbs and inhibitors which potently neutralize the pro-inflammatory phenotype from COVID-19 can partly relieve inflammation and CSS in the lung. Overall, we constructed a biosecurity animal model which mimics the cytokine storms and the pathophysiological changes in the patients with COVID-19 and as such can contribute to the mechanism study and therapeutic methods screening. We also identified some neutralizing mAbs and inhibitors have some prophylactic efficacy for COVID-19. More importantly, it could have useful implications for the intervention of existing or future coronavirus infectious diseases.

Results

Poly I:C and SARS-Cov-2 spike protein (SP) induced ARDS mice model

To determine whether the Poly I:C and SARS-Cov-2 SP could mimic SARS-Cov-2 caused ARDS and CSS, we inoculated Poly I:C and SP (SARS-Cov-2 mimic) into mice lung directly through intratracheal injection (Figure 1A). After installation of Poly I:C and SP, obvious acute lung injury featuring neutrophilic inflammation and interstitial edema was observed and the lung tissue showed increasingly severe injury with time (Figure 1B). Further histological analysis of the lungs confirmed the pathology induced by SARS-Cov-2 mimic, not Poly I:C or spike protein of SARS-Cov-2. Intratracheal instillation of SARS-Cov-2 mimic into mice resulted in lung injury at 24 h, to better understand the time course of pathologic changes in this mice model, we explored the time point of lung injury in this model. The

lung injury occurs around 6 and 24 h but not 48 h (Figure 1B). In addition, the mice suffered from extensive pleural fluid accumulation between 24 and 48 h post-challenge. Pleural effusion measured using by small animal MRI. Similar results were observed in small animal MRI captured image of the lung with gross lung lesions being observed at 24 h after challenge, reduced at 48 h, and not obvious at 6 h (Figure 1C).

Cytokine profile in Poly I:C and SP induced ARDS

In order to understand the mechanism of Poly I:C and SP induced lung injury in the molecular pathology, cytokines profile and flow cytometric analysis were performed to determine the inflammatory signaling molecules and related immune cells. Administration of the SARS-Cov-2 mimic resulted in an inflammatory cell influx into lung. Moreover, the influx of inflammatory cells being an indicator of lung inflammation.

In our SARS-Cov-2 mimic animal model, a single element neither SP nor Poly I:C can induce the IL-1α, IL-6 and TNFα burst featured CSS, compare with Poly I:C and SP group. Intratracheal instillation of the same volume of saline, SP and recombinant FC protein cannot stimulate the cytokines IL-1α, IL-6 and TNFα; However, installation of same volume and concentrations of Poly I:C shows increasing level of IL-1α and IL-6, but not TNFα (Figure 2A). Intratracheal injection of saline, SP and recombinant FC protein cannot stimulate increase of dsDNA, an indicator of NETs (Figure 2B). In our study, the dosage of 5 μg, 10 μg and 15 μg of SP in Poly I:C were tested in this model. There was a significant increase in total cellularity in the mice BAL samples and in a SP dose-dependent manner after 24 h challenge, with 15 μg of SP in Poly I:C showing the highest cellularity in the mice BAL samples (Figure 2C). Further investigation of cellularity in the mice BAL samples by flow cytometry, mouse GR-1 and F4/80 were labeled by antibody for neutrophils and macrophages with the

results showing that neutrophils, but not macrophages, significantly increased their infiltration and migration into the lungs. It should be noted that the number of neutrophils in the BAL at SP dose-dependent increased compared with saline (Figure 2D). The SARS-Cov-2 mimic led to an increase in the inflammatory cytokines IL-1α, IL-6 and TNFα. Specifically, these cytokines were significantly increased after the challenge, and at 6 h timepoint, they had burst, with TNFα and IL-6 being later significantly reduced by the 24 h timepoint. However, when compared with saline, all still had increased by 24 h timepoint (Figure 2E). We noted that there is no significant difference in the mice BAL samples between these two timepoint (Figure 2F). Moreover, a unique mechanism of neutrophil effector is generation of neutrophil extracellular traps (NETs), quantitation of NETs can be detected by measuring cell-free double-stranded DNA (dsDNA). In our study, we used the concentrations of dsDNA as indicator the NETs. At the 6 or 24 h timepoint after challenge, we noted that there is no significant difference in concentrations of dsDNA in the mice BAL samples (Figure 2G).

When the 6 h timepoint were compared with the 24 h timepoint, the cytokines were reduced, but there were no significant changes in the number of neutrophils and concentrations of dsDNA. However, to investigate the pro-inflammatory of cytokine responses, we dissociated the mice lung tissue into single cells after 24 h instillation of Poly I:C and SP, and maintained for 6 h and 24 h. The concentrations of IL-6 were still increasing after dissociation, and longer maintaining produce more IL-6 into the medium. This indicated that CSS happens in the lungs after instillation of SARS-Cov-2 with immune cells such as tissue-resident macrophages already being highly pro-inflammatory and activated (Figure 2H).

mAbs treatment of COVID-19 ARDS

We hypothesized that one or more cytokines IL-1α, IL-6, and TNFα drove the CSS induced ARDS in the lung. To test the hypothesis, we applied the neutralizing or blocking antibody via i.p. anti-IL-1α, anti-IL6R and anti-TNFR2 monoclonal antibodies. Neutralizing IL-1α directly reduced the production of IL-1α, and also indirectly reduced the production of IL-6 in BAL with no effect on TNFα (Figure 3A). Blocking of IL-6R by antibody can block cis and trans-signaling transduction of IL-6. However, treatment by IL-6R blocking antibody cannot alter the cytokines IL-1α, IL-6 and TNFα (Figure 3B). TNF exerts its effect by stimulation of two different receptors, TNFR1 and TNFR2, which work together and trigger distinct and common highly interconnected signaling pathways. TNFR1 is expressed in all cell types, but TNFR2 is only expressed in certain cell types, such as myeloid cells, glial cells and T and B cell subsets. We first tried to block TNFR2 and the NF-κB signaling in immune cells subset during the SARS-Cov-2 mimic challenge. Our results indicate that the blocking of TNFR2 cannot reduce the production of IL-1α, IL-6 and TNFα in BAL sample (Figure 3C). The percent of neutrophils in the BAL sample determined by a flow cytometric analysis. The percent of neutrophils after anti-IL-1α (Figure 3D), anti-IL6R (Figure 3E) and anti-TNFR2 (Figure 3F) indicate that blocking the IL-6R may reduce the infiltration of neutrophils. The concentrations of dsDNA during antibodies treatment did not reduce the NETs in mouse model (Figure 3G). To validate activities of the neutralizing or blocking antibodies, we performed RAW264.7 stimulated by Poly I:C and determined the effect by the production of IL-6 in the medium. The results indicate a reduced production of IL-6 while treating with 20 μg antibodies although not significantly (Figure 3H). Histological analysis results indicated that anti-IL-1α, anti-IL6R and anti-TNFR2 treatment all decrease the neutrophilic

inflammation and interstitial edema in the lung (Figure 3I). Neutralize or blocking antibodies of inflammatory cytokines reduced the production of inflammatory cytokine directly, beneficial effects of IL-1α, IL6R and TNFR2 blockade on SARS-Cov-2 induced lung injury in mice were observed. Potent therapeutic efficacy in a synergistic fashion can be considered in clinical.

Chemoprevention of COVID-19 ARDS

NETs can also be generated by macrophages[16], and strongly contribute to acute lung injury during virus infection[17-19]. We considered the hypothesis that the SARS-Cov-2 mimic stimulate the macrophages and produce inflammatory cytokine, such as IL-1α, IL6 and TNF-α, recruit and activate neutrophils via cytokines. Outbreak of cytokines contribute to the ARDS, blocking the downstream signaling pathway may reduce the ARDS under the challenge of SARS-Cov-2 mimic.

P38 and ERK are the signaling mediator of formation of NETs. MPO and Elastase as the peroxidase enzyme in neutrophils and essential for the formation of NETs[20,21]. TLR3/dsRNA complex inhibitor can block the interactions between TLR3 and Poly I:C. JAK inhibitor can block the IL-6 signaling pathway. Blocking of each cytokines signaling element may provide protection from ARDS. In our study, we have tried several small molecule inhibitors blocking the essential signaling pathways or a subset of immune cells. We noticed that the inhibition of P38 also reduces IL-1α in BAL and inhibition of JAK reduces IL-6 significantly with respect to the cytokine profiles of IL-1α, IL-6, and TNFα (Figure 4A). The percent of infiltrated neutrophils in the BAL sample was determined by a flow cytometric analysis. We saw the percent of infiltrated neutrophils being significantly reduced after treatment of P38, ERK and MPO inhibitors. The three inhibitors all targeted activities of neutrophils (Figure 4B). There is no significant difference of the concentrations of dsDNA during the treatment of inhibitors between the treated and untreated groups (Figure 4C). We performed the cell assay to

validate the effect of TLR3/dsRNA inhibitor and JAK inhibitors on mouse primary macrophages. TLR3/dsRNA inhibitor reduces the IL-6 production at 45 μM although not significantly, due to the IC50 of TLR3/dsRNA inhibitor was too high, a higher dose of this inhibitor required for further study. We saw that the JAK1/2 inhibitor Baricitinib can reduce the production of IL-6 significantly in a dose-dependent manner, but JAK2 inhibitor Febratinib cannot alter the production of IL-6 on mouse primary macrophages (Figure 4D). Histological analysis result indicated that inhibitors of P38, ERK, MPO and JAK inhibitor Baricitinib obviously decreasing the neutrophilic inflammation and interstitial edema in the lung, when to compared with the independent control group (Figure 4E).

Discussion

In order to understand the molecular mechanism of SARS-Cov-2 induced ARDS/CSS and find an effective strategy to prevent and remedy this highly infectious disease, establishing a SARS-Cov-2 pneumonia animal model is critical and necessary. Here, we have developed such SARS-Cov-2 murine ARDS model. We used Poly I:C to mimic the effect of viral RNA to stimulate the TLR3 signaling. Comparatively, it was reported that coronavirus includes a large genomic RNA and can stimulate TLR3 upon infection[22-26].

We named the combination of treatment of SARS-Cov-2 SP and Poly I:C as SARS-Cov-2 mimic. the unique outcome of recombinant SARS-Cov-2 spike protein in a TNFα outbreak featured cytokines storm when compared with Poly I:C challenged mice. The TNFα storm revealed the mechanism of CSS in COVID-19 patients, not just IL-6 and IL-1 but TNFα may play a more critical than others. Another feature that should be acknowledged is the TNFα burst after 6 h administration of Poly I:C and SP-ECD that later disappears in 24 h. Furthermore, IL-6 keeps its high level during the administration of SARS-Cov-2 mimics. However, SP-ECD of SARS-Cov-2 entry to cells though the

angiotensin-converting enzyme-related carboxypeptidase (ACE2) receptor[27]. Clear data indicate the critical role of ACE2 signaling pathway in the pathogenesis induced by SARS-Cov-2 SP.

CSS was found to be the major cause of morbidity in patients with SARS-CoV and MERS-CoV[28], with the presence of interleukin-6 (IL-6) in the serum being a hallmark of severe infections. IL-6 and IL-6 receptor in the serum are also significantly elevated in clinical features of SARS-Cov-2 severe patients[5]. Moreover, The CRP expression in COVID-19 patient which driven by IL-6 shows strongly correlated with COVID-19 severe patient survival[29]. Clinical trials using IL-6 and IL-6R antagonists are underway. IL-6R antagonist may suppress all IL-6 related cytokines signaling as well as trans presentation. the antagonist of IL-6 can suppress only cis and trans-signaling. downstream signal transduction of IL-6 is mediated by JAK-STAT3[30]. IL-6 can signal through two main pathways, cis signaling or trans-signaling in immune cells. Specifically, membrane-bound IL-6 receptor (mIL-6R) can bind to IL-6 and form a complex with gp130 and then transduction mediates by JAK-STAT3. But most cells can express gp130 and not mIL-6R. Therefore, in trans-signaling, soluble IL-6R (sIL-6R) bind with IL-6, then the IL-6-IL-6R complex bind with gp130 to activating the JAK-STAT3 signaling pathway. Cells that are activated by IL-6 in this manner do not express mIL-6R and will create a systemic cytokine storm. In our research, we first tested the IL-6R blocking antibody, blocking the trans and canonical presentation of the IL-6 signaling pathway. After administration of SARS-Cov-2 mimic, cytokines in BALF such as IL-1α, IL-6 and TNFα was not affected. Importantly, a reduced neutrophil infiltration was observed which merits attention despite the lack of statistically significant. This result may indicate the outcomes of anti-IL-6R blocking antibody, but dsDNA level shows the anti-IL-6R cannot prevent the SARS-Cov-2 mimics induced lung injury. We also applied the signaling inhibitors of JAK-STAT3, FDA approved JAK inhibitors Baricitinib and Fedratinib in our animal model,

Baricitinib is a selective JAK1 and JAK2 inhibitor. We found that, Baricitinib can decrease the IL-6 in lung BALF, indicating that the blocking of JAK-STAT3 signaling can inhibit the IL-6 mediated signaling transduction. In the cell assay, we established the Poly I:C viral mimic to stimulate primary macrophages. Treatment of Baricitinib in cell assay can decrease the production of IL-6 induced by Poly I:C. However, Fedratinib did not show the alteration in this assay. Fedratinib is a selective inhibitor of JAK2 with the IC50 of Fedratinib and Baricitinib being similar. Thus, we propose that blocking JAK1 can inhibit the production of IL-6 in primary mouse macrophages, but not blocking JAK2, JAK1 may be necessary in IL-6 signaling transduction during the ALI.

Impaired inflammatory responses in severe COVID-19 patients provide a distinct pattern of COVID-19 progression in host immune response to the SARS-Cov-2 infection, with pneumonia, lymphopenia, exhausted lymphocytes, high neutrophil to lymphocyte ratio, high production of IgG and a cytokine storm all being observed in severe cases of COVID-19[12,31-34]. Both the innate and adaptive immune responses to control the virus infection are necessary, but whether protective or pathogenic host response remains to be determined. Importantly, the dysregulated host response impairs the tissue and less contribute to anti-viral response[12,35]. Here we used the neutralizing or blocking antibodies, essential pathway inhibitors of the innate and adaptive immune responses to target to the most abundant cytokines, NETs and other proinflammatory factors to prevent the SARS-Cov-2 caused CSS and ARDS.

The pathophysiology of high pathogenicity for SARS-Cov-2 remains unclear, our data indicate that potential combination of those neutralizing/blocking antibodies or inhibitors may contribute to the treatment of CSS and ARDS, and should be investigated further. Early reports from clinical notice the proinflammatory cytokines in serum including GCSF, IP10, MCP1, MIP1A, and TNF were associated

with pulmonary inflammation and acute lung injury. Other research suggests the key role for monocytes and macrophages in the bronchoalveolar fluid (BALF) and that two chemokines CCL2 and CCL7 play an important role for the development of diseases in the severe COVID-19 patients. Recruitment of CC-chemokine receptor 2- positive (CCR2+) monocytes play a potent role in patients mortality[36]. Single-cell sequencing data indicated that macrophages in the lungs may contribute to inflammation by producing multiple cytokines/chemokines, and recruiting more inflammatory monocytic cells and neutrophils. Macrophages in patients with moderate COVID-19 tend to generate more T cell-engaging chemokines CXCR3 and CXCR6 [36,37]. This different pattern of lung-resident macrophages may drive the pathogenicity of the host response to SARS-Cov-2 infection. We have applied various signal pathway inhibitors to block the dysregulated macrophages and neutrophils. TLR3/dsRNA Complex Inhibitor blocked the dsRNA and TLR3 receptor interaction directly, but due to the involvement of viral protein, cytokines profile already changed, and the pattern of lung injury may be altered. To prevent sustained activation of neutrophils, we applied P38 inhibitor SB203580, ERK inhibitor Tauroursodeoxycholate and MPO inhibitor 4-Aminobenzoic hydrazide in the SARS-Cov-2 mimic model. It was reported that MPO is a functional and activation marker of neutrophils. Elastase was produced by neutrophils and can mediate lung injury. Inhibitors of MPO and elastase can directly reduce the acute lung injury at the inflammatory site[21,38,39]. In our study, inhibitors targeting neutrophils include P38 inhibitor, ERK inhibitor, MPO inhibitor and elastase inhibitor can reduce the neutrophil infiltration into lung, but not elastase, but single inhibitor may offer no protection from SARS-Cov-2 viral mimic induced pathogenesis of ARDS, and as such multiple inhibitors may need to be simultaneously utilized. During the process of neutrophil activation, neutrophil extracellular

traps (NETs) are released which consists of DNA/Histone 1 backbones and various pro-inflammatory proteins against virus infection, but dysregulation of NETs produces substantial lung injury[40,41].

SARS-Cov-2 has posed a serious threat to global public health. Antiviral drugs, such as hydroxychloroquine, chloroquine and remdesivir did not achieve an ideal therapeutic effect[42,43]. Approaches that neutralize the virus or block viral infection process can lead a developed vaccine and treatment to the immunopathology of COVID-19 as it provides different approaches to support the patients of COVID-19[31,44]. By using Poly I:C and SP, we established a murine robustness model for research of COVID-19 caused CSS, address the immunopathology alterations, and explore new therapies of COVID-19. Our model can be safety used for the molecular mechanism study, drug discovery, and target finding for SARS-Cov-2 induced ARDS/CSS.

Methods and material

Experimental Animals

Male BALB/c mice (8-10 weeks) free of pathogens were purchased from Beijing Vital River Laboratory Animal Technology Co., Ltd. (Beijing, China). Mice were housed in a pathogen-free environment under conditions of 20C° ± 2C°, 50% ± 10% relative humidity, 12-h light/dark cycles. They were provided with food and water *ad libitum.* All experimental procedures involving animals were approved by the Ethics Review Commission of Zhengzhou University (following internationally established guidelines).

COVID-19 ARDS murine model and treatment

Mice were anesthetized via intraperitoneal (IP) injection with Pentobarbital Sodium (50 mg/kg). A small incision was made over the trachea, and the underlying muscle and glands were separated to

expose the trachea. Male mice (BALB/c strain, 8-10 weeks) were intratracheally administered with freshly mixed Poly I:C (Poly I:C-HMW, Invivogen, tlrl-pic) 2.5 mg/ml and SARS-Cov-2 recombinant spike protein (ECD-His-tag, Genescript, Z03481) 15 μg (in saline), followed by 100 μL air. 2.5 mg/kg Poly I:C, FC control, 15 μg SARS-Cov-2 recombinant spike protein and saline was administered intratracheally Independent at the same volume as control.

Blocking and neutralizing antibodies anti-IL-1α (InVivoMab, BE0243), IL-6R (InVivoMab, BE0047), and TNFR2 (InVivoMab, BE0247) were administrated intraperitoneally as a single dose of 200 μg 24 h prior. TLR3/dsRNA inhibitor (Merck, 614310) was dissolved in DMSO at 100 mg/ml stock, administrated via i.p. at 50 mg/kg 2 h prior to installation of SARS-Cov-2 mimics. MPO inhibitor (Merck, A41909) was dissolved in DMSO at 200 mg/kg, administrated via i.p. at 50 mg/kg per day, 3 d prior to installation of SARS-Cov-2 mimics. P38 inhibitor (MCE, HY-10256) was dissolved in DMSO at 80 mg/kg, administrated via i.p. at 20 mg/kg per day, 3 d prior to installation of SARS-Cov-2 mimics. ERK inhibitor (MCE, HY-19696A) was dissolved in DMSO at 400 mg/kg, administrated via i.p. at 100 mg/kg per day, 3 d prior to installation of SARS-Cov-2 mimics. Elastase Inhibitor (GLPBIO, GC11981) was dissolved in DMSO at 20 mg/kg, administrated via i.p. at 5 mg/kg per day, 3 d prior to installation of SARS-Cov-2 mimics. JAK inhibitor (MCE, HY-15315) as dissolved in DMSO at 80 mg/kg, administrated via i.p. at 20 mg/kg per day, 3 d prior to installation of SARS-Cov-2 mimics.

Analysis of BALF samples

6 h after the administration, mice were anesthetized via intraperitoneal (IP) injection of Pentobarbital Sodium 50 mg/kg. A 26G venous indwelling needle hose was inserted into the exposed tracheal lumen, and then the airway was washed three times with 1 ml saline each, the first lavage fluid sample is kept separately to test cytokines.

Multiplex cytokines assay

Bronchoalveolar lavage fluid (BALF) was collected from mice lung after executed, the mice BALF were separated by centrifuge and store at -80℃. BALF sample collection was performed as previously described. Next, concentrations of mice Inflammatory related cytokines IL-1α, IL-1β, IL-6, IL-10, IL-12p70, IL-17A, IL-23, IL-27, MCP-1, IFN-β, IFN-γ, TNF-α, and GM-CSF were measured by LEGENDplex™ Mouse Inflammation Panel (13-plex, Biolegend), the data harvest by flow cytometry using FACSCalibur (BD).

Flow Cytometry analysis

Fluorescent labeled antibodies were performed to quantify neutrophils and macrophages. Unconjugated anti-mouse CD16/CD32 (Biolegend, 101320) was used for blocking Fc receptors, APC labeled anti-mouse Ly-6G/Ly-6C (Gr-1) and FITC labeled anti-mouse F4/80 were performed for neutrophils and macrophages, incubate 30 m on ice, protect from light. Wash three times by PBS and centrifuged to remove the supernatant and responded in 150 μL PBS. Samples were analyzed in the BD FACSCalibur (BD).

Histopathology and Immunohistochemistry Analysis

An independent experiential was performed for the histopathology analysis of pulmonary. The mouse lungs were removed intact and weighted, then fixed in 10% formalin and paraffin-embedded. Three different fields were selected from a lung section and three sections per animal were evaluated, 3 μm sections were cut on a Leica model rotary microtome and stained with hematoxylin-eosin. Histological analysis was subjected by two independent pathologists blindly.

Paraffin sections (3-μm thick) were obtained from the mice lung as described below. anti-DNA/Histone H1 antibody (Merck, MAB3864) was used for quantitation of neutrophil extracellular traps (NETs) of neutrophils at a dilution of 1:200, Alexa Fluor 633 goat anti-mouse (Life Technologies, Carlsbad, CA) was performed for secondary staining. Fluorescence intensity was analyzed using Image-Pro Plus software.

Mouse macrophage cell culture

RAW264.7 cell was cultured in DMEM medium supplemented with penicillin (100 units/mL), streptomycin (100 μg/mL), and 10% FBS (Biological Industries, Kibbutz Beit-Haemek, Israel).

Compounds treated to RAW264.7

RAW264.7 cell (6×10^5 cells/well) was seeded into 12-well plates and cultured for 24 h in the incubator. Diluted Poly I:C in blank DMEM medium to reach a final concentration of 10 μg/ml, then, make a series dilution of compound X in blank DMEM medium which contained 10 μg/ml Poly I:C and treated to the RAW264.7 cell in the 12-well plate. Meanwhile, RAW264.7 cell was changed to blank DMEM medium with or without Poly I:C as a positive or negative control. The cells were maintained at 37°C in a 5% CO_2 incubator for 12 h, harvested the supernatant for the detection of IL-6 secretion.

Mouse primary macrophage cell culture

Carefully took out the bone from the mouse and removed the muscle and connective tissues on the bone. They were washed the containing in the bone out by DPBS using 1 ml Syringe. Suspended the eluate and centrifuged at 1000 rpm for 5 m. Washed the pellets by DPBS and resuspended the cell pellets by RPMI-1640 containing penicillin(100 units/mL), streptomycin (100 μg/mL), 10% FBS (Biological Industries, Kibbutz Beit-Haemek, Israel) and 50 ng/ml M-CSF (peprotech), plated the cells

in a low attachment culture dish and maintained at a 5% CO_2 incubator. Changed the cells with a fresh complete RPMI-1640 contained 50 ng/ml M-CSF every other day until the density of adherent cells reached 90%. Digested the cells and plated 6×10^5 cells/well into 12-well plates, cultures for 24 h and treated the Poly I:C and compound to the cell using blank RPMI-1640 medium. This method is similar to the treatment of RAW264.7.

Dissociated of primary lung cells mix

Took out the whole lung tissues of the mice and washes by pre-cold PBS containing DNase I (0.01 mg/ml) (Sigma), penicillin (100 units/mL), and streptomycin (100 μg/mL). Tattered the lung tissues into small pieces in a sterile centrifuge tube by scissors, suspended the small pieces by 1 mg/ml Type I collagenase (Sigma) supplied by 0.01 mg/ml DNase I and digested in a 37℃ shaking incubator for 30 min. Filtered the solution with a 200 mesh sieve and centrifuged at 1000 rpm for 5 min, subsequently. After washed the pellets twice by pre-cold PBS containing DNase I (0.01 mg/ml), resuspended the pellets by RPMI-1640 containing 10% FBS (Biological Industries, Kibbutz Beit-Haemek, Israel) and seeded into 12-well plate. Harvested the supernatant after 24 h culture and removed the floating cells by centrifuge at 3000 rpm for 5 m. The ELISA was performed to detect the IL-6 concentration as the manufacture's protocol.

Statistical Analysis

Statistical analysis was performed using GraphPad Prism 7.0 (GraphPad Software, United States). Specific statistical methods and comparisons made by methods as described in figure legend. Comparison between two groups were performed by paired Student t-test or unpaired Student t-test. p

< 0.05 was regarded as statistically significant and marked with a star, data is reported as mean ± SEM, and error bars indicate SEM.

Reference

1 Wang, C., Horby, P. W., Hayden, F. G. & Gao, G. F. A novel coronavirus outbreak of global health concern. *Lancet* **395**, 470-473, doi:10.1016/S0140-6736(20)30185-9 (2020).

2 Zhu, N. *et al.* A Novel Coronavirus from Patients with Pneumonia in China, 2019. *N Engl J Med* **382**, 727-733, doi:10.1056/NEJMoa2001017 (2020).

3 Wu, F. *et al.* A new coronavirus associated with human respiratory disease in China. *Nature* **579**, 265-269, doi:10.1038/s41586-020-2008-3 (2020).

4 Lu, R. *et al.* Genomic characterisation and epidemiology of 2019 novel coronavirus: implications for virus origins and receptor binding. *Lancet* **395**, 565-574, doi:10.1016/S0140-6736(20)30251-8 (2020).

5 Huang, C. *et al.* Clinical features of patients infected with 2019 novel coronavirus in Wuhan, China. *Lancet* **395**, 497-506, doi:10.1016/S0140-6736(20)30183-5 (2020).

6 Tortorici, M. A. & Veesler, D. Structural insights into coronavirus entry. *Adv Virus Res* **105**, 93-116, doi:10.1016/bs.aivir.2019.08.002 (2019).

7 Hoffmann, M. *et al.* SARS-CoV-2 Cell Entry Depends on ACE2 and TMPRSS2 and Is Blocked by a Clinically Proven Protease Inhibitor. *Cell* **181**, 271-280 e278, doi:10.1016/j.cell.2020.02.052 (2020).

8 Chen, N. *et al.* Epidemiological and clinical characteristics of 99 cases of 2019 novel coronavirus pneumonia in Wuhan, China: a descriptive study. *Lancet* **395**, 507-513, doi:10.1016/S0140-6736(20)30211-7 (2020).

9 An, P. J., Yi, Z. Z. & Yang, L. P. Biochemical indicators of coronavirus disease 2019 exacerbation and the clinical implications. *Pharmacol Res*, 104946, doi:10.1016/j.phrs.2020.104946 (2020).

10 Xu, Z. *et al.* Pathological findings of COVID-19 associated with acute respiratory distress syndrome. *Lancet Respir Med* **8**, 420-422, doi:10.1016/S2213-2600(20)30076-X (2020).

11 Oberfeld, B. *et al.* SnapShot: COVID-19. *Cell* **181**, 954-954 e951, doi:10.1016/j.cell.2020.04.013 (2020).

12 Qin, C. *et al.* Dysregulation of immune response in patients with COVID-19 in Wuhan, China. *Clin Infect Dis*, doi:10.1093/cid/ciaa248 (2020).

13 Tan, M. *et al.* Immunopathological characteristics of coronavirus disease 2019 cases in Guangzhou, China. *Immunology*, doi:10.1111/imm.13223 (2020).

14 Neerukonda, S. N. & Katneni, U. A Review on SARS-CoV-2 Virology, Pathophysiology, Animal Models, and Anti-Viral Interventions. *Pathogens* **9**, doi:10.3390/pathogens9060426 (2020).

15 Sun, S. H. *et al.* A Mouse Model of SARS-CoV-2 Infection and Pathogenesis. *Cell Host Microbe*, doi:10.1016/j.chom.2020.05.020 (2020).

16 Boe, D. M., Curtis, B. J., Chen, M. M., Ippolito, J. A. & Kovacs, E. J. Extracellular traps and macrophages: new roles for the versatile phagocyte. *Journal of leukocyte biology* **97**,

1023-1035 (2015).
17 Liu, S. *et al.* Neutrophil extracellular traps are indirectly triggered by lipopolysaccharide and contribute to acute lung injury. *Scientific reports* **6**, 37252 (2016).
18 Narasaraju, T. *et al.* Excessive neutrophils and neutrophil extracellular traps contribute to acute lung injury of influenza pneumonitis. *The American journal of pathology* **179**, 199-210 (2011).
19 Lefrançais, E., Mallavia, B., Zhuo, H., Calfee, C. S. & Looney, M. R. Maladaptive role of neutrophil extracellular traps in pathogen-induced lung injury. *JCI insight* **3** (2018).
20 Zhao, X. *et al.* Neutrophils undergo switch of apoptosis to NETosis during murine fatty liver injury via S1P receptor 2 signaling. *Cell Death & Disease* **11**, 1-14 (2020).
21 Pulavendran, S. *et al.* Production of Neutrophil Extracellular Traps Contributes to the Pathogenesis of Francisella tularemia. *Front Immunol* **11**, 679, doi:10.3389/fimmu.2020.00679 (2020).
22 Law, H. K. *et al.* Toll-like receptors, chemokine receptors and death receptor ligands responses in SARS coronavirus infected human monocyte derived dendritic cells. *BMC immunology* **10**, 35 (2009).
23 Vercammen, E., Staal, J. & Beyaert, R. Sensing of viral infection and activation of innate immunity by toll-like receptor 3. *Clinical microbiology reviews* **21**, 13-25 (2008).
24 Enjuanes, L. *et al.* Molecular Basis of Coronavirus Virulence and Vaccine Development. *Adv Virus Res* **96**, 245-286, doi:10.1016/bs.aivir.2016.08.003 (2016).
25 Mazaleuskaya, L., Veltrop, R., Ikpeze, N., Martin-Garcia, J. & Navas-Martin, S. Protective role of Toll-like Receptor 3-induced type I interferon in murine coronavirus infection of macrophages. *Viruses* **4**, 901-923, doi:10.3390/v4050901 (2012).
26 Totura, A. L. *et al.* Toll-Like Receptor 3 Signaling via TRIF Contributes to a Protective Innate Immune Response to Severe Acute Respiratory Syndrome Coronavirus Infection. *mBio* **6**, e00638-00615, doi:10.1128/mBio.00638-15 (2015).
27 Yan, R. *et al.* Structural basis for the recognition of SARS-CoV-2 by full-length human ACE2. *Science* **367**, 1444-1448 (2020).
28 Channappanavar, R. & Perlman, S. Pathogenic human coronavirus infections: causes and consequences of cytokine storm and immunopathology. *Semin Immunopathol* **39**, 529-539, doi:10.1007/s00281-017-0629-x (2017).
29 Yan, L. *et al.* An interpretable mortality prediction model for COVID-19 patients. *Nature Machine Intelligence*, 1-6 (2020).
30 Kang, S., Tanaka, T., Narazaki, M. & Kishimoto, T. Targeting interleukin-6 signaling in clinic. *Immunity* **50**, 1007-1023 (2019).
31 Cao, X. COVID-19: immunopathology and its implications for therapy. *Nat Rev Immunol* **20**, 269-270, doi:10.1038/s41577-020-0308-3 (2020).
32 Zhang, B. *et al.* Immune phenotyping based on neutrophil-to-lymphocyte ratio and IgG predicts disease severity and outcome for patients with COVID-19. *medRxiv* (2020).
33 Chen, X. *et al.* Restoration of leukomonocyte counts is associated with viral clearance in COVID-19 hospitalized patients. *MedRxiv* (2020).
34 Zheng, M. *et al.* Functional exhaustion of antiviral lymphocytes in COVID-19 patients. *Cellular & molecular immunology*, 1-3 (2020).
35 Wen, W. *et al.* Immune cell profiling of COVID-19 patients in the recovery stage by

single-cell sequencing. *Cell discovery* **6**, 31, doi:10.1038/s41421-020-0168-9 (2020).

36 Liao, M. *et al.* Single-cell landscape of bronchoalveolar immune cells in patients with COVID-19. *Nature Medicine*, 1-3 (2020).

37 Cao, X. COVID-19: immunopathology and its implications for therapy. *Nature reviews immunology* **20**, 269-270 (2020).

38 Antonelou, M. *et al.* Therapeutic Myeloperoxidase Inhibition Attenuates Neutrophil Activation, ANCA-Mediated Endothelial Damage, and Crescentic GN. *J Am Soc Nephrol* **31**, 350-364, doi:10.1681/ASN.2019060618 (2020).

39 Okeke, E. B. *et al.* Inhibition of neutrophil elastase prevents neutrophil extracellular trap formation and rescues mice from endotoxic shock. *Biomaterials* **238**, 119836, doi:10.1016/j.biomaterials.2020.119836 (2020).

40 Chand, H. S., Muthumalage, T., Maziak, W. & Rahman, I. Pulmonary toxicity and the pathophysiology of electronic cigarette, or vaping product, use associated lung injury. *Frontiers in pharmacology* **10** (2019).

41 Hook, J. S. *et al.* Nox2 Regulates Platelet Activation and NET Formation in the Lung. *Front Immunol* **10**, 1472, doi:10.3389/fimmu.2019.01472 (2019).

42 Wang, Y. *et al.* Remdesivir in adults with severe COVID-19: a randomised, double-blind, placebo-controlled, multicentre trial. *The Lancet* (2020).

43 Molina, J. M. *et al.* No evidence of rapid antiviral clearance or clinical benefit with the combination of hydroxychloroquine and azithromycin in patients with severe COVID-19 infection. *Med Mal Infect* **10** (2020).

44 Vabret, N. *et al.* Immunology of COVID-19: current state of the science. *Immunity* (2020).

Figure Legend

Figure 1: SARS-Cov-2 mimic induced acute lung injury in BALB/c mice. (A) A schematic description of Poly I:C and SARS-Cov-2 spike protein intratracheal administration in mice. (B) Histological characteristics of lung injury and interstitial pneumonia induced by Poly I:C and SARS-Cov-2 spike protein (Poly I:C+S); 6 h, 24 h and 48 h after challenge. Control group; Saline and Poly I:C 24 h challenge. Bar=100 μm (C) In vivo small animal MRI documented pleural effusion induced by Poly I:C and SARS-Cov-2 spike protein; 6 h, 24 h and 48 h after challenge. Control group; Saline and Poly I:C 24 h challenge.

Figure 2: SARS-Cov-2 mimic induced cytokines release storm in lung. (A) Production of IL-6 in the BAL from SARS-Cov-2 mimic challenged mice, $^{**}p<0.01$, $^{***}p<0.001$. (B) Levels of dsDNA in the BAL from SARS-Cov-2 mimic challenged mice, $^{***}p<0.001$, ns. (C) Total cell count in the BAL from Poly I:C and 5 μg, 10 μg or 15 μg SARS-Cov-2 spike challenged mice, control group; Saline. $^{*}p<0.05$, $^{**}p<0.01$, $^{***}p<0.001$. 6 h or 24 h after SARS-Cov-2 mimic challenged mice. Control group; Saline (D) Cellular composition in BALF, $^{*}p<0.05$. (E) BALF IL-6 concentration. $^{*}p<0.05$, $^{**}p<0.01$, $^{***}p<0.001$, ns. (F) Cellular composition in BAL, $^{**}p<0.01$, $^{***}p<0.001$, ns. (G) Levels of dsDNA in the BAL. $^{*}p<0.05$, $^{***}p<0.001$, ns. Single cells dissociated from SARS-Cov-2 mimic challenged mice lung (H) IL-6 concentration from cell culture medium, $^{***}p<0.001$.

Figure 3: Blocking of inflammatory cytokines. (A) BALF IL-6, IL-1α and TNFα concentrations from anti-IL-1α treated mice. $^{*}p<0.05$, $^{**}p<0.01$, ns. (B) BALF IL-6, IL-1α and TNFα concentrations from anti-IL-6R treated mice. (C) BALF IL-6, IL-1α and TNFα concentrations from anti-TNFR2 treated mice. (D, E and F) Cellular composition in BALF, anti-IL-1α, anti-IL-6R or anti-TNFR2 treated mice. (G) Levels of dsDNA in the BAL. Poly I:C stimulate the IL-6 production in mouse macrophages (H) IL-6 concentration from cell culture medium. (I) Histological characteristics of lung injury and interstitial pneumonia. Bar=100 μm

Figure 4: Blocking of inflammatory related signaling pathways. (A) BALF IL-6, IL-1α and TNFα concentrations. $^{*}p<0.05$. (B) Percent of neutrophils in BAL. $^{*}p<0.05$. (C) Levels of dsDNA in the BAL. Poly I:C stimulate the IL-6 production in mouse primary macrophages (D) IL-6 concentration from cell culture medium. $^{*}p<0.05$.ns. (E) Histological characteristics of lung injury and interstitial pneumonia. Bar=100 μm.

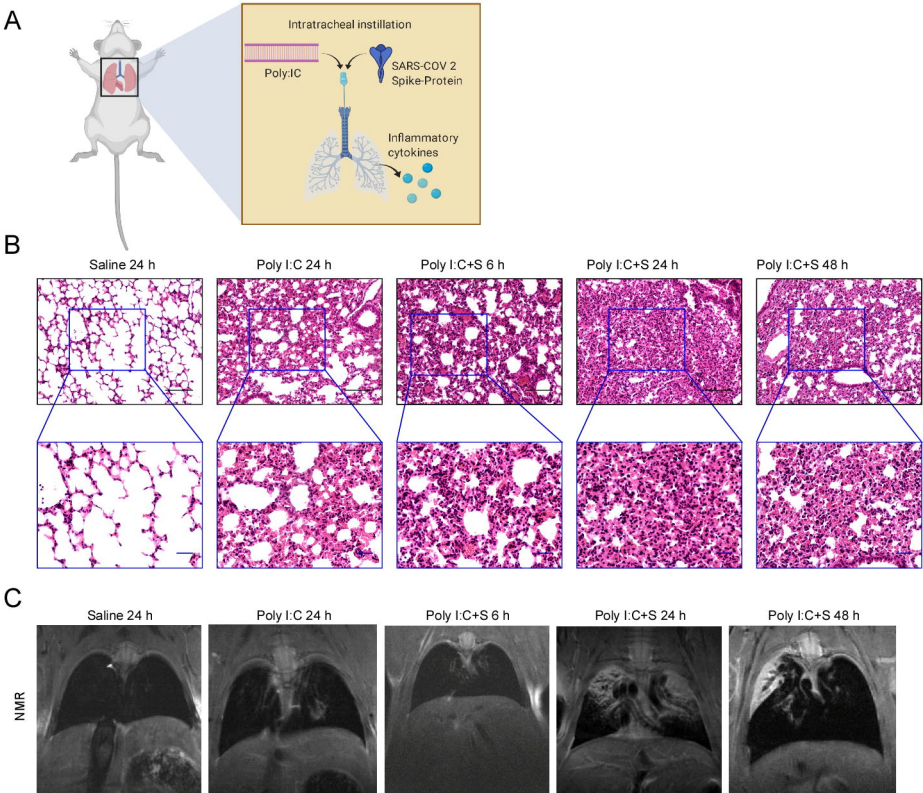
A
Intratracheal instillation
Poly:IC
SARS-COV 2
Spike-Protein
Inflammatory
cytokines
B
Saline 24 h
Poly I:C 24 h
Poly I:C+S 6 h
Poly I:C+S 24 h
Poly I:C+S 48 h
C
Saline 24 h
Poly I:C 24 h
Poly I:C+S 6 h
Poly I:C+S 24 h
Poly I:C+S 48 h
NMR

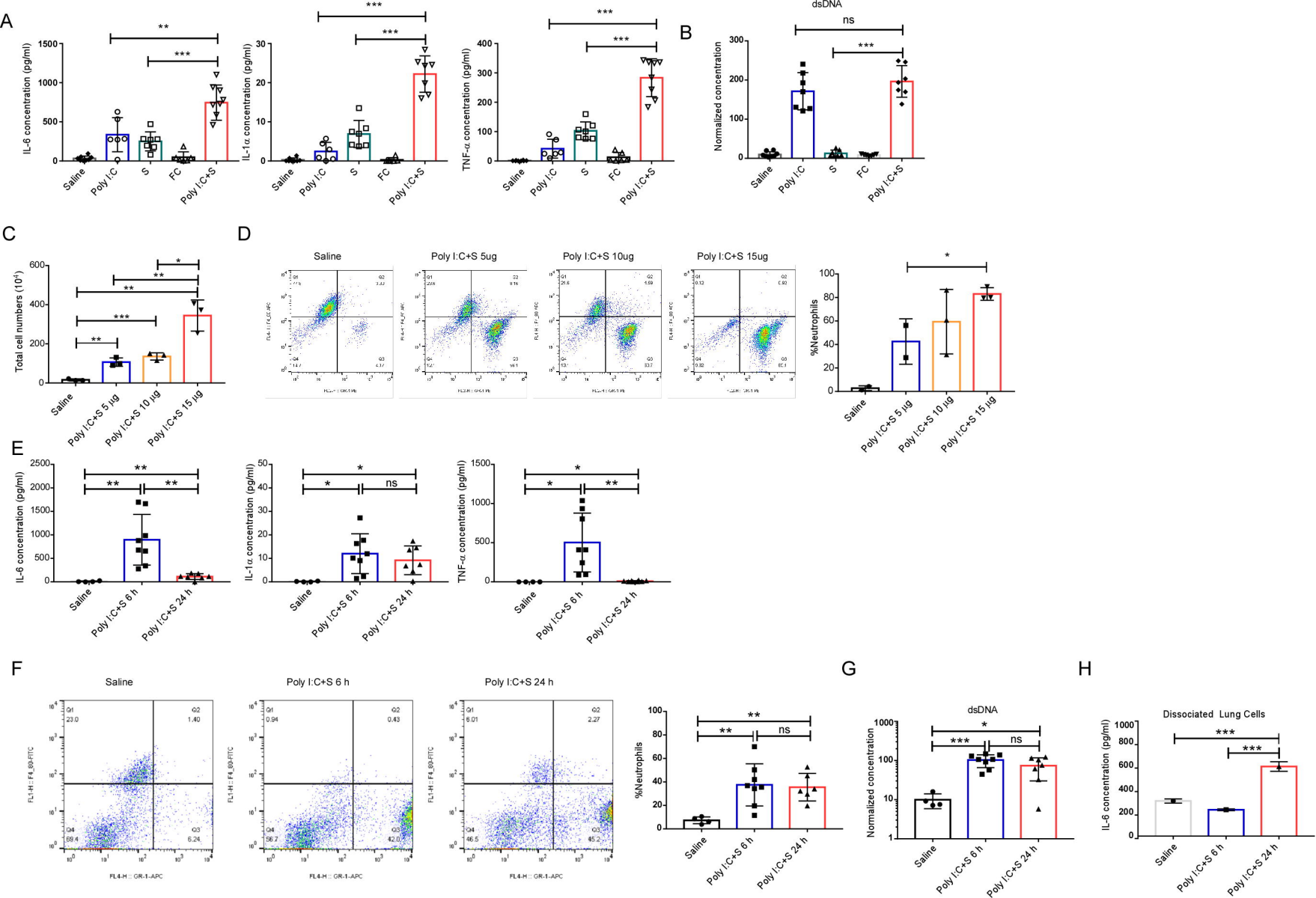
A
IL-6 concentration (pg/ml)
IL-1α concentration (pg/ml)
TNF-α concentration (pg/ml)
Saline
Poly I:C
S
FC
Poly I:C+S
B
dsDNA
Normalized concentration
ns
C
Total cell numbers (10⁴)
Poly I:C+S 5 μg
Poly I:C+S 10 μg
Poly I:C+S 15 μg
D
Saline
Poly I:C+S 5ug
Poly I:C+S 10ug
Poly I:C+S 15ug
%Neutrophils
E
Poly I:C+S 6 h
Poly I:C+S 24 h
F
Poly I:C+S 6 h
Poly I:C+S 24 h
G
H
Dissociated Lung Cells

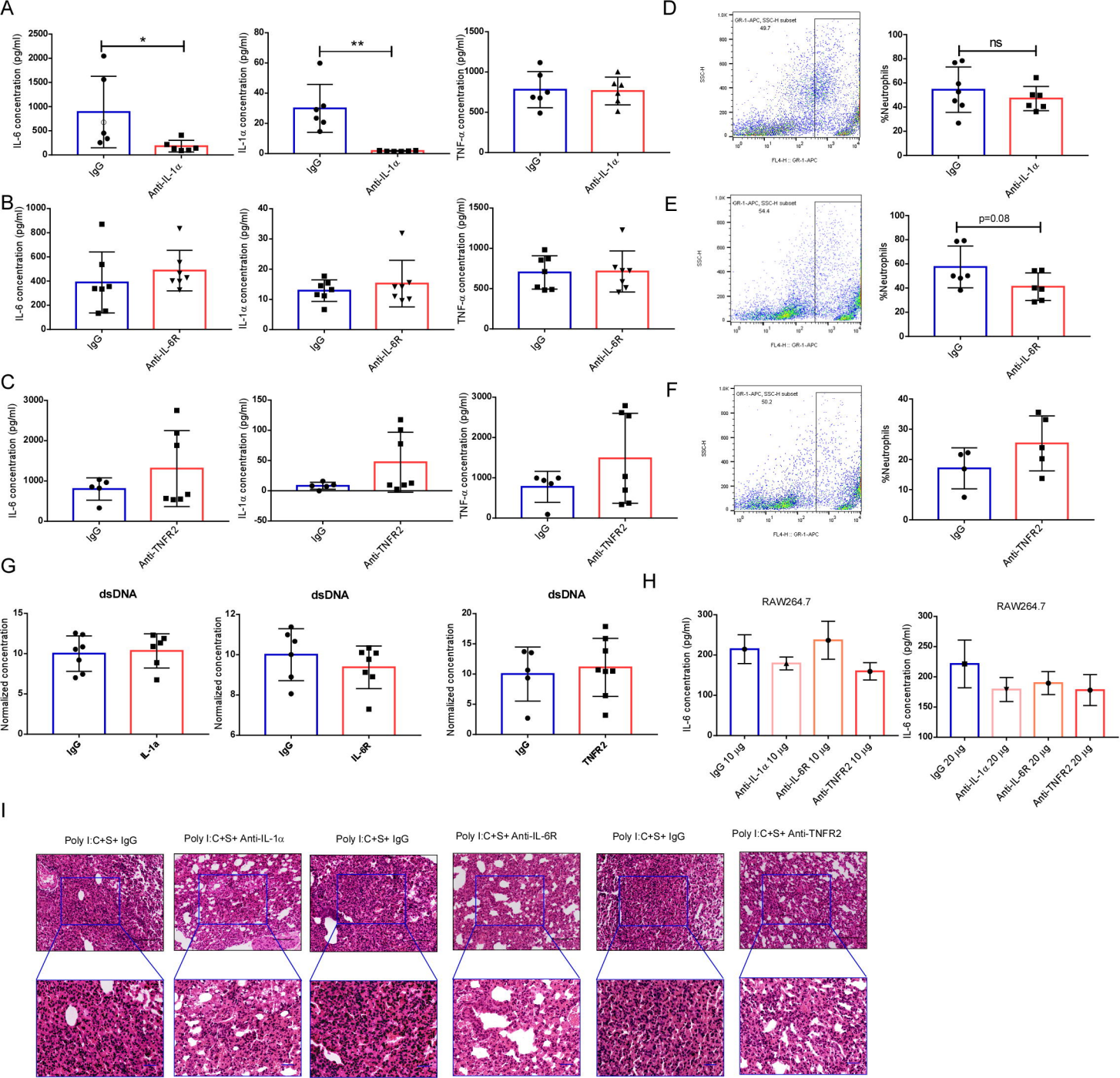
A
IL-6 concentration (pg/ml)
IL-1α concentration (pg/ml)
TNF-α concentration (pg/ml)
IgG
Anti-IL-1α
*
**
B
Anti-IL-6R
C
Anti-TNFR2
D
GR-1-APC, SSC-H subset
49.7
SSC-H
FL4-H :: GR-1-APC
%Neutrophils
ns
E
54.4
p=0.08
F
50.2
G
dsDNA
Normalized concentration
IL-1a
IL-6R
TNFR2
H
RAW264.7
IgG 10 μg
Anti-IL-1α 10 μg
Anti-IL-6R 10 μg
Anti-TNFR2 10 μg
IgG 20 μg
Anti-IL-1α 20 μg
Anti-IL-6R 20 μg
Anti-TNFR2 20 μg
I
Poly I:C+S+ IgG
Poly I:C+S+ Anti-IL-1α
Poly I:C+S+ IgG
Poly I:C+S+ Anti-IL-6R
Poly I:C+S+ IgG
Poly I:C+S+ Anti-TNFR2

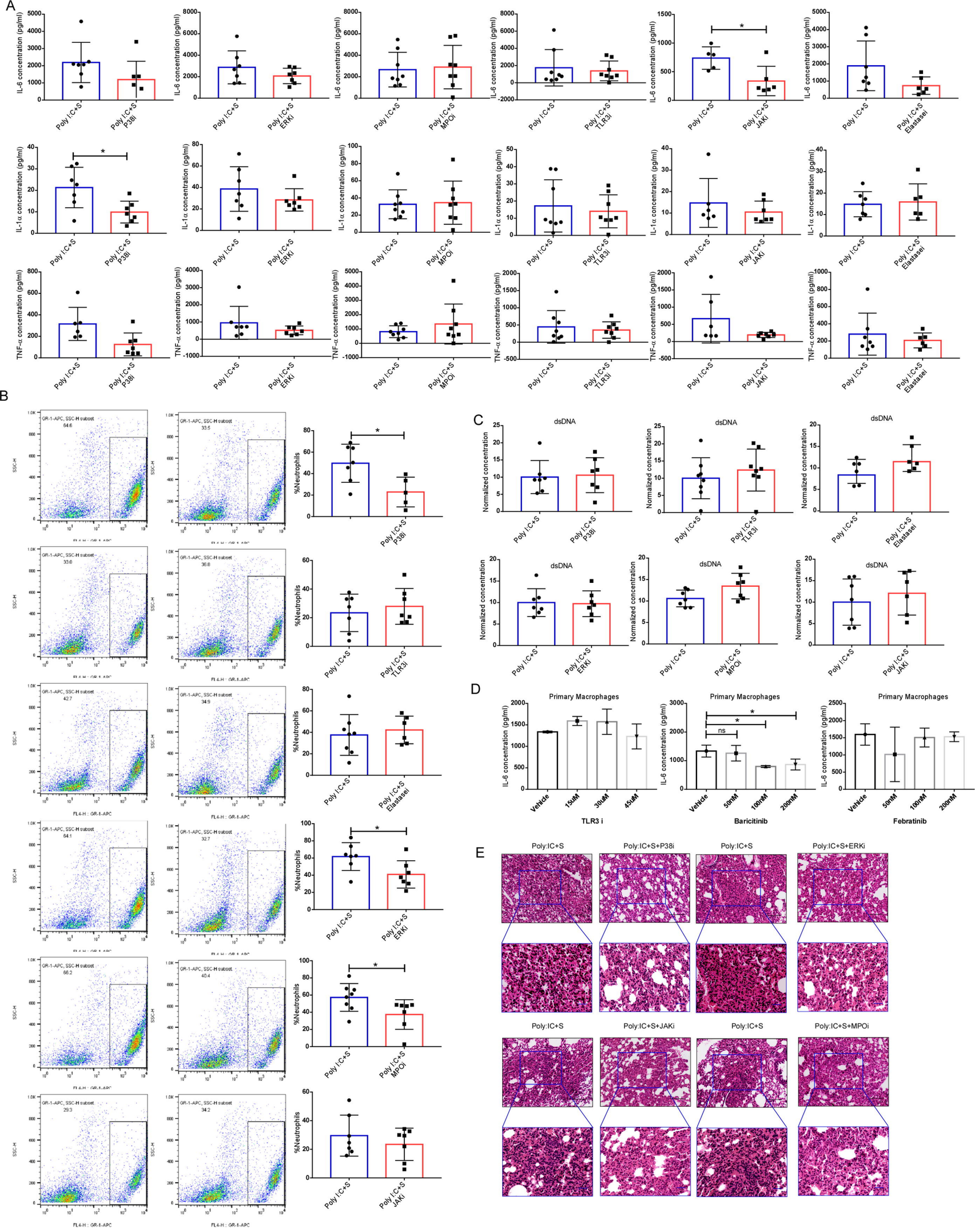
A
IL-6 concentration (pg/ml)
IL-1α concentration (pg/ml)
TNF-α concentration (pg/ml)
Poly I:C+S
Poly I:C+S P38i
Poly I:C+S ERKi
Poly I:C+S MPOi
Poly I:C+S TLR3i
Poly I:C+S JAKi
Poly I:C+S Elastasei
B
GR-1-APC, SSC-H subset
SSC-H
FL4-H :: GR-1-APC
%Neutrophils
C
dsDNA
Normalized concentration
D
Primary Macrophages
IL-6 concentration (pg/ml)
Vehicle
15uM
30uM
45uM
TLR3 i
50nM
100nM
200nM
Baricitinib
Febratinib
ns
E
Poly:IC+S
Poly:IC+S+P38i
Poly:IC+S+ERKi
Poly:IC+S+JAKi
Poly:IC+S+MPOi